HETEROGENEOUS CHARACTERIZATION OF COMPOSITE MATERIALS WITH PROGRESSIVE DAMAGE

Final Report

by

I. M. Daniel
J. D. Achenbach
L. M. Keer

Center for Quality Engineering and Failure Prevention
Northwestern University
Evanston, IL 60208

for

Air Force Office of Scientific Research
Bolling AFB, DC 20332

June 1991

(U)
CURITY CLASSIFICATION OF THIS PAGE

REPORT DOCUMENTATION PAGE

a. REPORT SECURITY CLASSIFICATION: Unclassified	1b. RESTRICTIVE MARKINGS
2a. SECURITY CLASSIFICATION AUTHORITY	3. DISTRIBUTION/AVAILABILITY OF REPORT: Unlimited
2b. DECLASSIFICATION/DOWNGRADING SCHEDULE	
4. PERFORMING ORGANIZATION REPORT NUMBER(S): C447-3	5. MONITORING ORGANIZATION REPORT NUMBER(S)
6a. NAME OF PERFORMING ORGANIZATION: Northwestern University; 6b. OFFICE SYMBOL (If applicable)	7a. NAME OF MONITORING ORGANIZATION: Air Force Office of Scientific Research (AFOSR)
6c. ADDRESS (City, State and ZIP Code): Evanston, IL 60208	7b. ADDRESS (City, State and ZIP Code): Bolling AFB, DC 20332 AFOSR/NA Bolling AFB DC 20332-6448
8a. NAME OF FUNDING/SPONSORING ORGANIZATION; 8b. OFFICE SYMBOL (If applicable)	9. PROCUREMENT INSTRUMENT IDENTIFICATION NUMBER: Grant No. AFOSR-88-0124
8c. ADDRESS (City, State and ZIP Code): AFOSR/NA Bolling AFB DC 20332-6448	10. SOURCE OF FUNDING NOS.

PROGRAM ELEMENT NO.	PROJECT NO.	TASK NO.	WORK UNIT NO.
61102F	2302/[redacted]	B2	

11. TITLE (Include Security Classification) "HETEROGENEOUS CHARACTERIZATION OF Composite Materials with Progressive Damage" (U)

12. PERSONAL AUTHOR(S): L. M. Daniel, J. D. Achenbach, L. M. Keer

13a. TYPE OF REPORT	13b. TIME COVERED	14. DATE OF REPORT (Yr., Mo., Day)	15. PAGE COUNT
Final	FROM 2/1/88 TO 1/31/91	1991/06/28	39

16. SUPPLEMENTARY NOTATION

COSATI CODES		
FIELD	GROUP	SUB. GR.

18. SUBJECT TERMS (Continue on reverse if necessary and identify by block number): Composite Materials; Micromechanics; Interphase; Ceramic-matrix Composites.

19. ABSTRACT (Continue on reverse if necessary and identify by block number)

The objective of this investigation is to develop constitutive and failure models for composite materials based on observed damage mechanisms and damage development. Unidirectional continuous-fiber ceramic-matrix composites were investigated under longitudinal and transverse loading. Failure mechanisms and their development were studied in real time under the microscope. Micromechanical analyses were conducted and stress distributions were obtained in the constituents and around matrix and interfacial cracks. The influence of the interphase region on stress-strain and failure properties was studied. A modified shear lag analysis yielded stress-strain behavior to failure and relations between applied stress, matrix cracking and fiber-matrix debonding.

20. DISTRIBUTION/AVAILABILITY OF ABSTRACT: CLASSIFIED/UNLIMITED ☒ SAME AS RPT. ☑ DTIC USERS ☑	21. ABSTRACT SECURITY CLASSIFICATION: Unclassified

22a. NAME OF RESPONSIBLE INDIVIDUAL	22b. TELEPHONE NUMBER (Include Area Code)	22c. OFFICE SYMBOL
~~I. M. Daniel~~ Steven Boyce	~~(708) 491-5649~~ 202 767-6963	AFOSR/NA

FORM 1473, 83 APR EDITION OF 1 JAN 73 IS OBSOLETE.

(U)
SECURITY CLASSIFICATION OF THIS PAGE

FORWARD

This is the Final Report on project "Heterogeneous Characterization of Composite Materials with Progressive Damage," prepared by Northwestern University for the Air Force Office of Scientific Research under Grant No. AFOSR-88-0124. The work described in this report was conducted in the period February 1, 1988 to January 31, 1991. Lt. Colonel Steven Boyce is the AFOSR project manager. Professors I. M. Daniel, J. D. Achenbach and L. M. Keer are principal investigators. Additional contributions to the work reported herein were made by Drs. E. E. Gdoutos, J. W. Lee, A. Wijeyewickrema and H. Zhu, and Messrs. G. Anastassopoulos, H. S. Choi and P. Van Heurck.

NORTHWESTERN UNIVERSITY

I. M. Daniel
Professor
Theoretical and Applied Mechanics

HETEROGENEOUS CHARACTERIZATION OF COMPOSITE MATERIALS WITH PROGRESSIVE DAMAGE

1. INTRODUCTION

The objective of this investigation is to develop constitutive and failure models for composite materials based on observed damage mechanisms and damage development. Ceramic-matrix composites were investigated under longitudinal and transverse tensile loading. Interrelated analytical and experimental studies were conducted as discussed below.

Four basic areas were investigated during this program:

1. Experimental Micromechanics of Brittle-Matrix Composites.
2. Analytical/Experimental Studies of Brittle-Matrix Composites under Longitudinal Tension.
3. Analytical Studies of Interphase Effects in Transversely Loaded Composite.
4. Failure Models for Unidirectional Composites under Longitudinal Tension.

The highlights and principal results from each of the above tasks are described below.

2. EXPERIMENTAL MICROMECHANICS OF BRITTLE-MATRIX COMPOSITES

2.1 Introduction

The objective of this task was to study failure mechanisms on a microscopic scale in a unidirectional ceramic matrix composite under longitudinal and transverse loading.

The material investigated was SiC/CAS calcium aluminosilicate reinforced with silicon carbide fibers (Corning Glass Works). The fiber is silicon carbide yarn known as Nicalon (Nippon Carbon Co.). The composite material was obtained in the form of 8-ply and 24-ply thick unidirectional plates and crossply laminates of $[0/90]_{2s}$ and $[0/90_2]_s$ layups.

The fiber and composite material were characterized to obtain physical and mechanical properties. Unidirectional specimens of the composite instrumented with strain gages were tested under longitudinal and transverse tensile loading in a servohydraulic testing machine to obtain average mechanical properties. Specimens instrumented with strain gages were also used to determine the coefficients of thermal expansion. Measured and literature properties of the constituent and composite materials are tabulated in Tables 1 and 2.

Table 1. Constituent Material Properties

Property	CAS Matrix	SiC Fiber
Maximum Use Temperature, °C (°F)	1350 (2460)	1300 (2370)
Fiber Diameter (μm)	-	15
Density (g/cm^3)	2.8	2.6
Coefficient of Thermal Expansion 10^{-6}/°C(10^{-6}/°F)	5.0 (2.8)	3.1 (1.7)
Elastic Modulus, GPa (10^6 psi)	98 (14.2)	163 (23.6)
Tensile Strength, MPa (ksi)	124 (18) (flexural)	1930 (280)

Table 2. Measured Properties of SiC/CAS Unidirectional Composite

Property	Value
Fiber Volume Ratio, V_f	0.39
Ply Thickness, t, mm (in.)	0.38 (0.015)
Longitudinal Modulus, E_1, GPa (Msi)	121 (17.6)
Transverse Modulus, E_2, GPa (Msi)	112 (16.2)
In-plane Shear Modulus, G_{12}, GPa (Msi)	44 (6.4)
Major Poisson's Ratio, ν_{12}	0.20
Longitudinal Tensile Strength, F_{1T} MPa (ksi)	435 (63)
Transverse Tensile Strength, F_{2T}, MPa (ksi)	22 (3.2)
Longitudinal Ultimate Tensile Strain, ε^u_{1T}	0.0085
Transverse Ultimate Tensile Strain, ε^u_{2T}	0.0002

Failure mechanisms were studied by testing unidirectional specimens under the microscope with a specially designed fixture [1,2]. Load is applied and controlled by means of a pneumatic cylinder. The specimen with the grips attached is mounted onto a reaction frame attached to one end of the pneumatic cylinder. One end of the specimen is connected to the moving piston while the other end is reacted at the other end of the reaction frame through a strain gage load cell. The entire assembly including air cylinder, reaction frame, specimen with grips and load cell, is suspended with counterweights from a movable upright frame.

2.2 Longitudinal Loading

Figure 1 shows a typical longitudinal stress-strain curve to failure. This curve displays several characteristic features which are related to the failure mechanisms and failure process. The initial region AB corresponds to the linear elastic behavior of the material prior to any significant microfailures. Region BC corresponds to transverse matrix crack initiation and multiplication up to a saturation density to be discussed below. This is followed by a quasi-linear region CD in which no further significant matrix damage takes place, and a final slightly steeper region DE. Fiber fractures and debonding which start before transverse matrix crack saturation continue until final failure. The terminal modulus is somewhat lower than the one predicted by assuming complete debonding. The difference may be due in part to fiber misalignment and partial fiber fractures.

The micromechanical behavior and failure mechanisms were studied by testing and observing specimens under the microscope. The first isolated transverse matrix cracks appeared above a stress level of 100 MPa (14.5 ksi), but significant matrix cracking started above a stress level of 180 MPa (26 ksi) corresponding to a strain of $\varepsilon_1 = 1.14 \times 10^{-3}$ which is very close to the ultimate tensile strain of the bulk matrix material. Figure 2 shows typical photomicrographs with transverse matrix cracking increasing in density with applied stress. A plot of applied stress versus crack density was superimposed on the average stress-strain curve for the material (Fig. 3). The crack density reaches a saturation level of 28 cracks/mm, or a minimum crack spacing of 36 μm (0.0014 in.). Thus, the minimum crack spacing appears to be on the order of two fiber diameters.

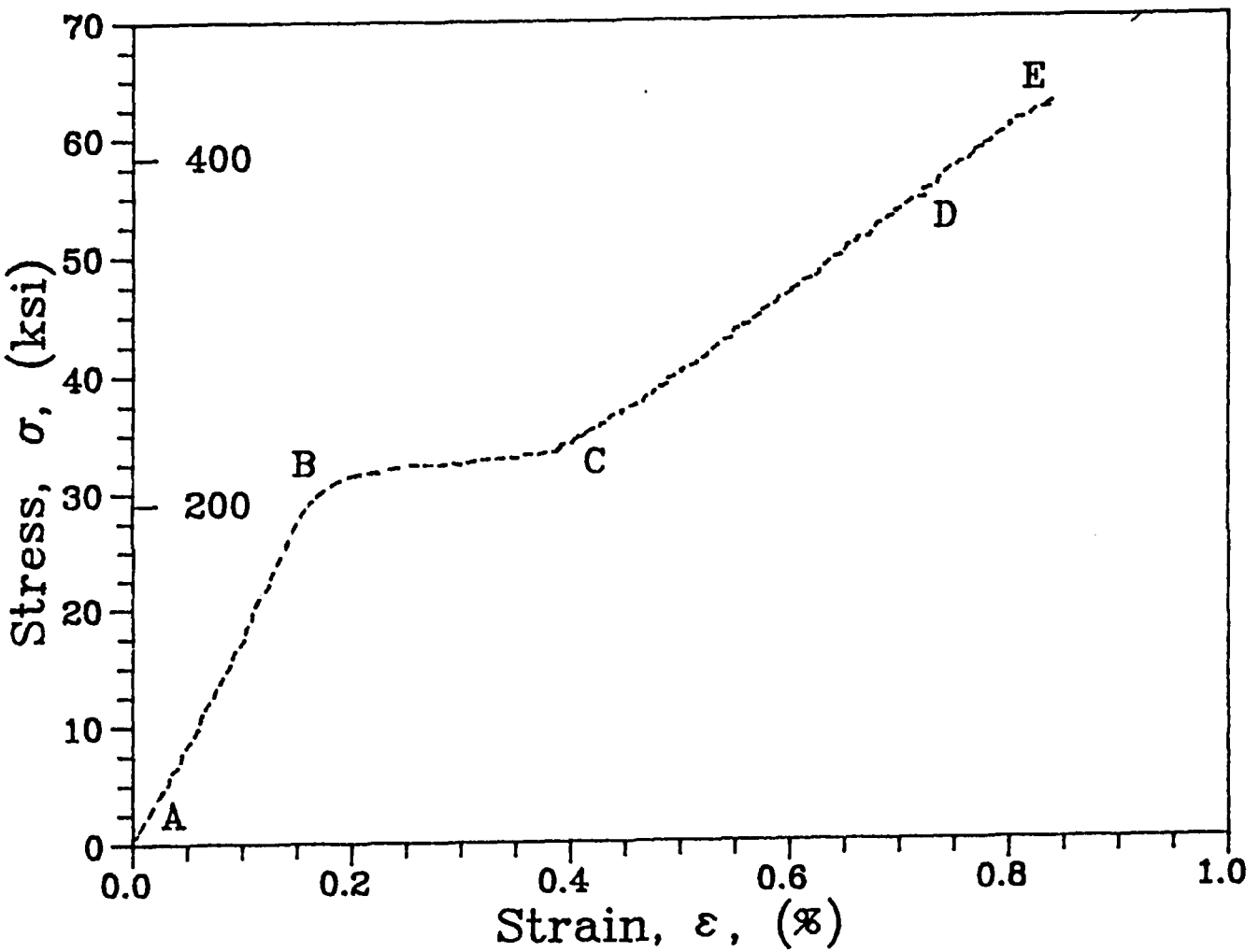

Fig. 1 Stress-Strain Curve for $[0_8]$ SiC/CAS Specimen under Uniaxial Tensile Loading

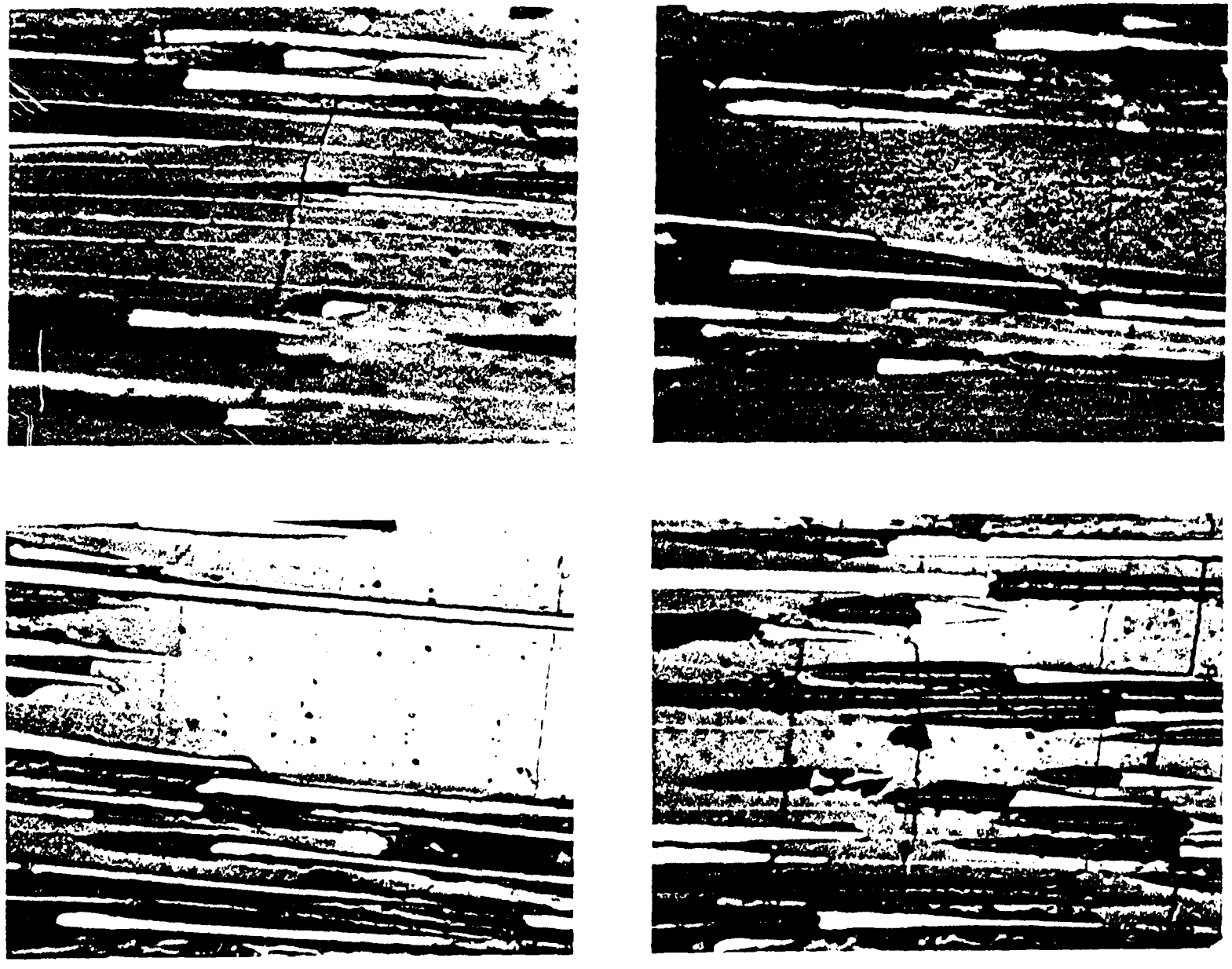

Fig. 2 Typical Photomicrographs Showing Initiation and Multiplication of Transverse Matrix Cracks Under Longitudinal Tensile Loading

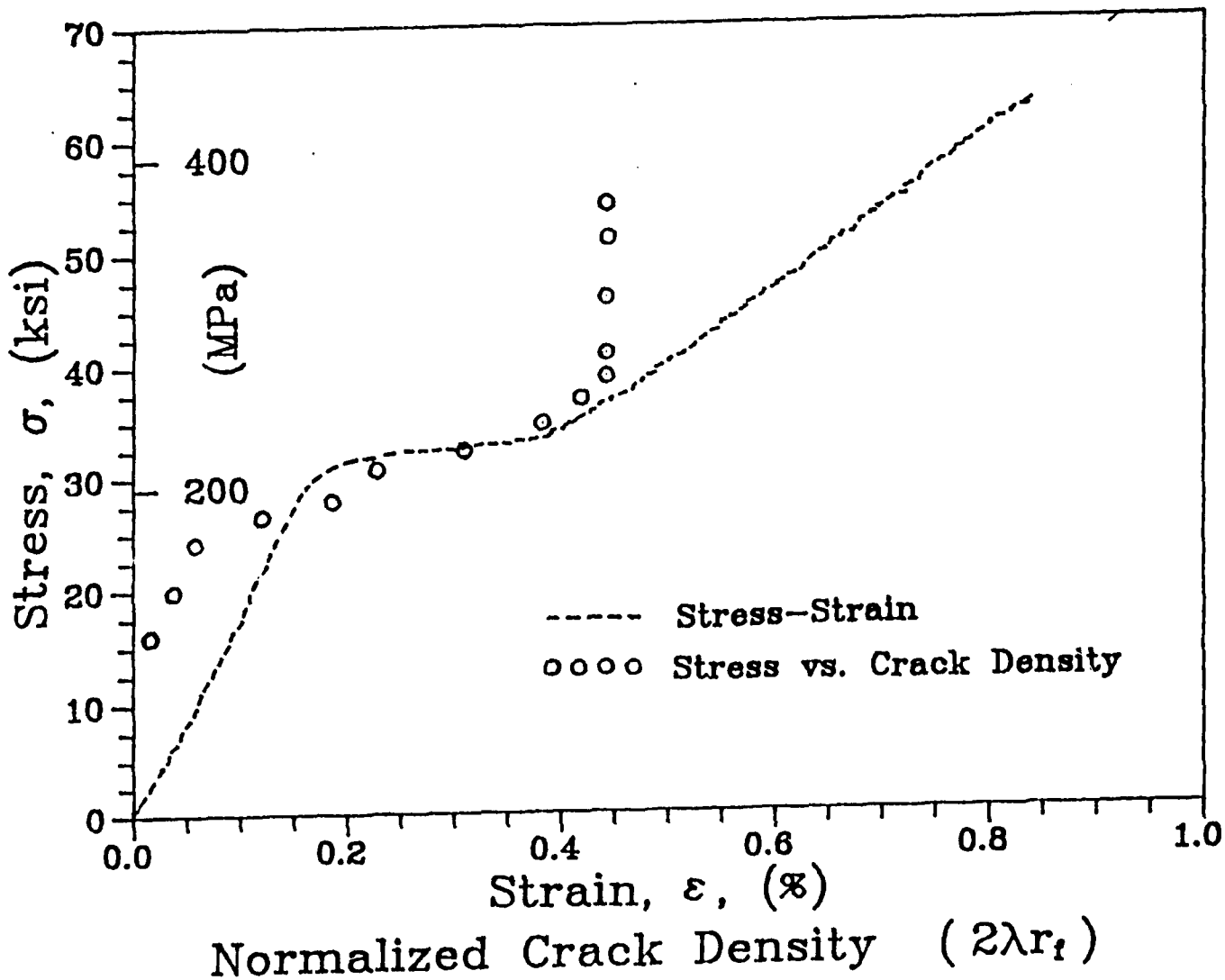

Fig. 3 Stress-Strain and Stress versus Crack Density Curves for $[0_8]$ SiC/CAS Specimen under Uniaxial Tensile Loading

Interfacial fiber-matrix debonding develops before matrix crack saturation, although its initiation and extent could not be pinpointed experimentally. Isolated fiber breaks were observed before matrix crack saturation and increased in frequency as the matrix cracks reached their maximum density (Fig. 4). Most fiber breaks occurred at a short distance, one to four fiber diameters, from the nearest matrix crack, possibly due to fiber-matrix debonding causing a local stress rise at the end of the debonded length (Fig. 5). As the load was increased the fiber cracks opened wider indicating further debonding and slippage.

At a high enough stress level, of approximately 345 MPa (50 ksi) in this case, no further cracking or fiber fracture was observed. It is possible, although not easy to confirm experimentally that total fiber-matrix debonding ensues leading to linear behavior in the last stage of the stress-strain curve.

2.3 Transverse Loading [1,2]

This is the most severe type of loading because of the low tensile strength of the matrix material and the high stress concentration at the fiber matrix interface. Stress distributions in the matrix can be obtained analytically and experimentally. Assuming that the in-situ properties of the constituent materials are well known and using an appropriate failure criterion, one can predict failure initiation. This usually takes place in the interphase region in the form of a short crack. Its location and orientation with respect to the fiber cross section depend on the relative elastic and ultimate properties of the matrix, fiber and interphase zone, and on the fiber packing and volume ratio.

Some average properties obtained from transverse tensile tests are shown in Table 2. Microscopic failure mechanisms were studied by testing specimens under the microscope. The first microcracks originated at the fiber-matrix interface and are nearly normal to the interface, which indicates that failure is caused by the circumferential tensile stress in the matrix. The randomness of the fiber packing makes it difficult to draw conclusions, however, some general patterns can be identified.

When the fibers are closely packed, usually in a near hexagonal array, radial cracks initiate

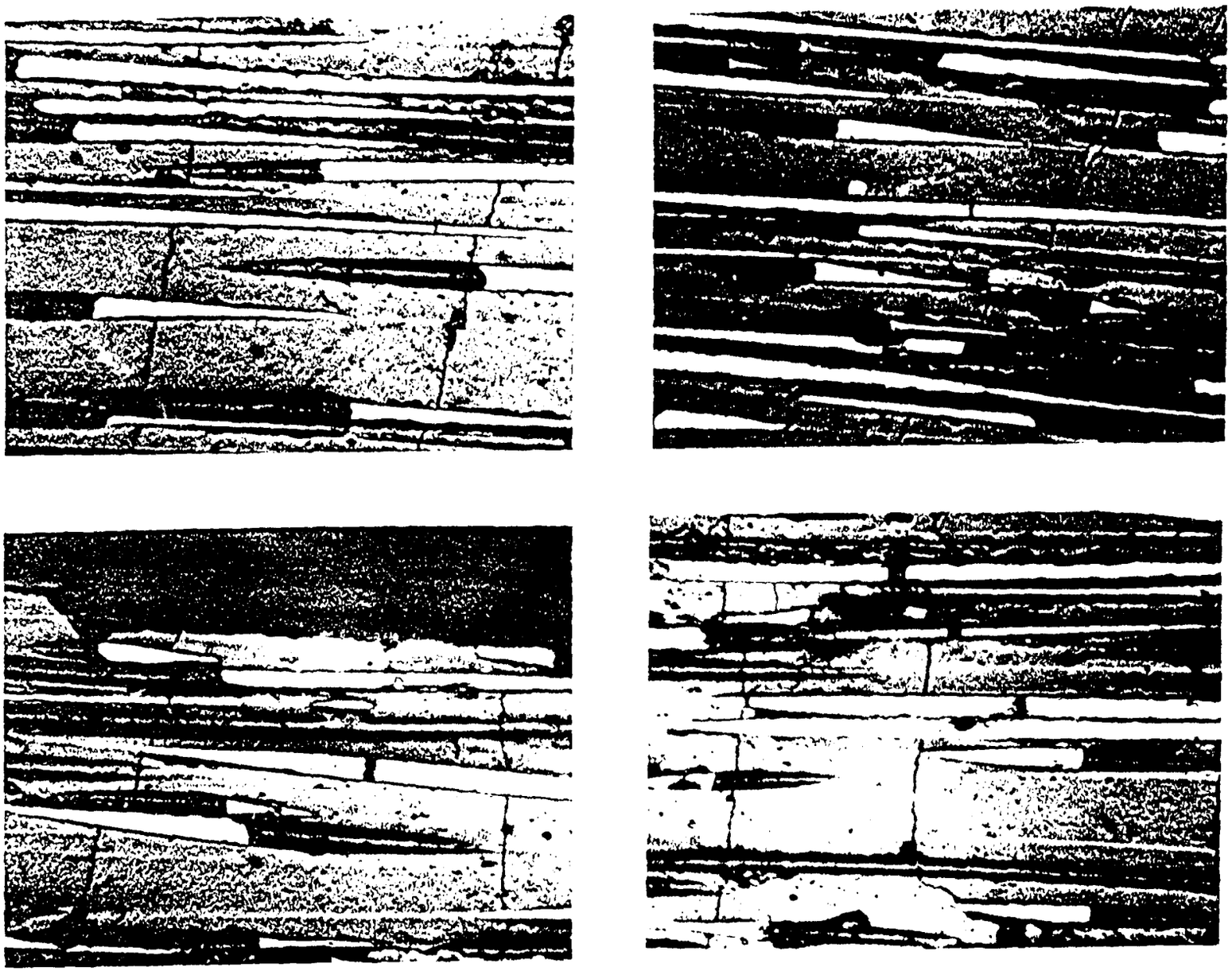

Fig. 4 Photomicrographs Illustrating Fiber Fractures and Fiber Crack Opening Between Matrix Cracks

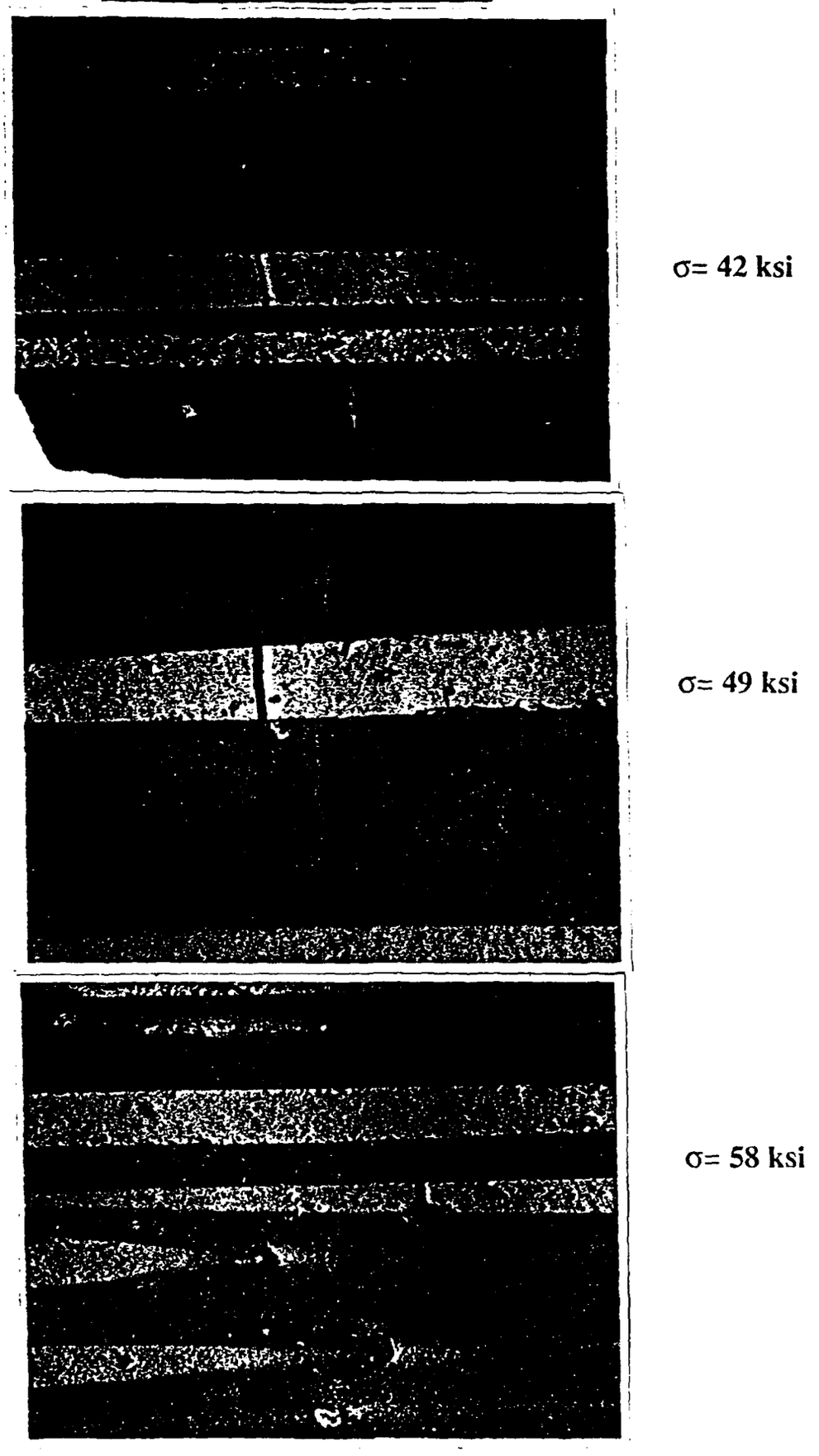

Fig. 5 Typical Fiber Fractures Near Matrix Cracks with Fiber-Matrix Debonding

at approximately 45° from the loading axis. When fibers are farther apart and are surrounded by a relatively large volume of matrix, radial cracks occur at approximately 90° from the loading axis (Fig. 6).

As the load increases a new failure mechanism develops, consisting of interface cracks in the area along the loading axis over an arc 2θ about the 0° point, with $\theta < 45°$ (Fig. 6). These interface cracks are not immediately connected to the radial cracks developed earlier. Additional radial cracks may develop in this second stage of damage development. In the third stage of damage development radial and interfacial cracks are connected to form a long continuous cracks. If there is no constraint, such as that provided by the 0° fibers in a crossply laminate, total failure ensues. The various failure mechanisms and stages of damage development, are illustrated schematically in Fig. 7.

The influence of the various failure mechanisms on the macroscopic stress-strain behavior of a crossply laminate is illustrated in Fig. 8. The appearance of the matrix radial cracks causes a sudden reduction in average stiffness. Thereafter, the laminate stiffness is stabilized until the occurrence of interfacial cracks, which cause another abrupt reduction in stiffness. The crack interconnections and formation of macrocracks cause further, albeit more gradual, stiffness reduction.

Some micromechanics analyses were conducted to explain the phenomena observed. The case of a fiber surrounded by a large volume of matrix can be approximated by that of an inclusion in an infinite medium and can be treated by classical elasticity. In this analysis the existence of a thin interphase region of lower (but unknown) modulus was assumed. Radial and circumferential stresses were computed in the matrix around the fiber for various values of the interphase region modulus (Fig. 9). The results show that for high interphase modulus, the radial stress at the 0° location is the most critical one, leading to interfacial cracking. However, for lower interphase moduli, the circumferential stress at the 90° location becomes critical, resulting in the observed radial cracks. A similar analysis for a closely packed hexagonal array of fibers showed that for a low stiffness interphase, the peak circumferential stress is the critical one and it occurs near the 45°

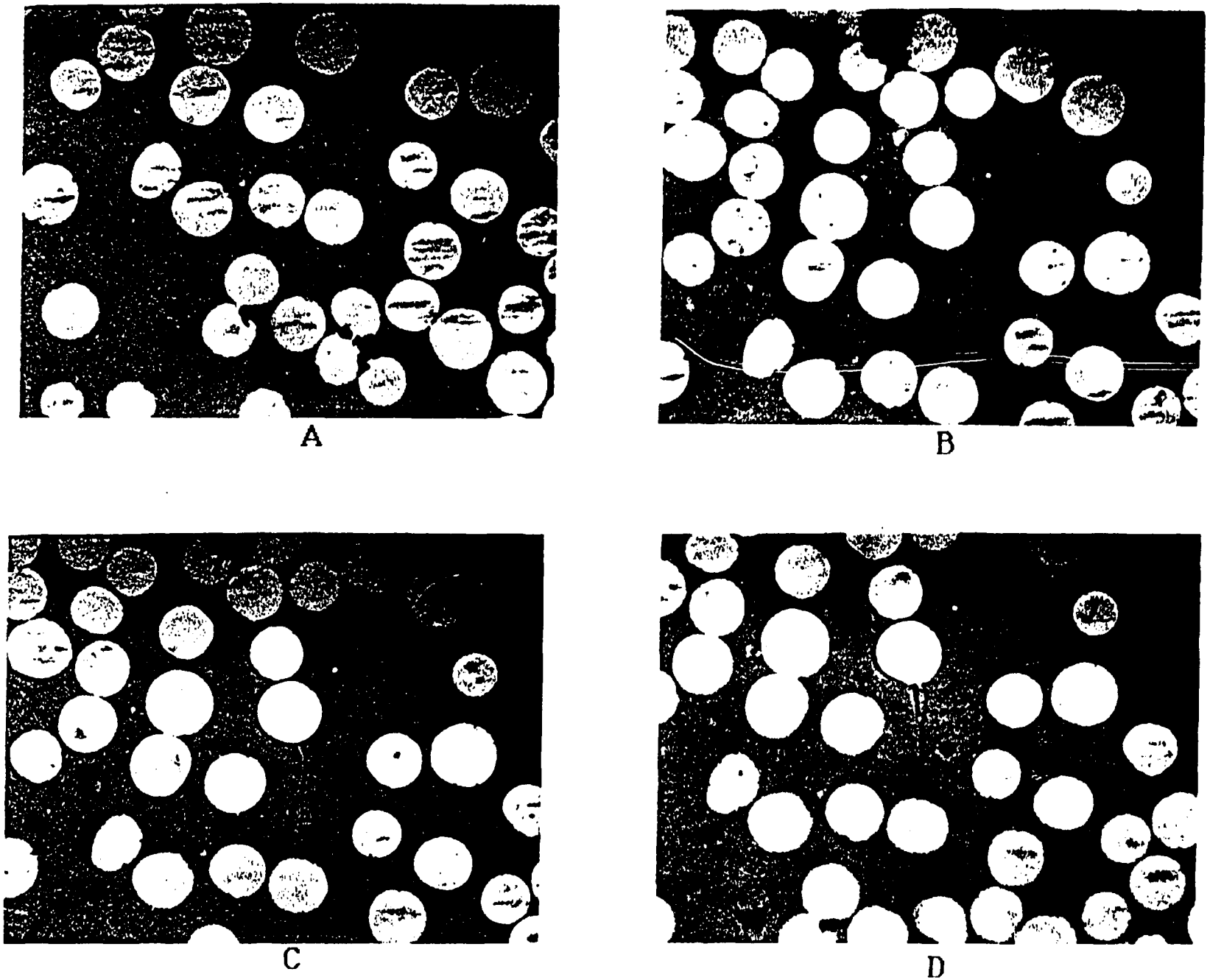

Fig. 6 Photomicrographs of failure mechanisms in [90_8] SiC/CAS specimen under transverse tensile loading, (a) undamaged material, (b) initial radial cracks, (c) radial and interfacial cracks, (d) interconnection of radial and interfacial cracks

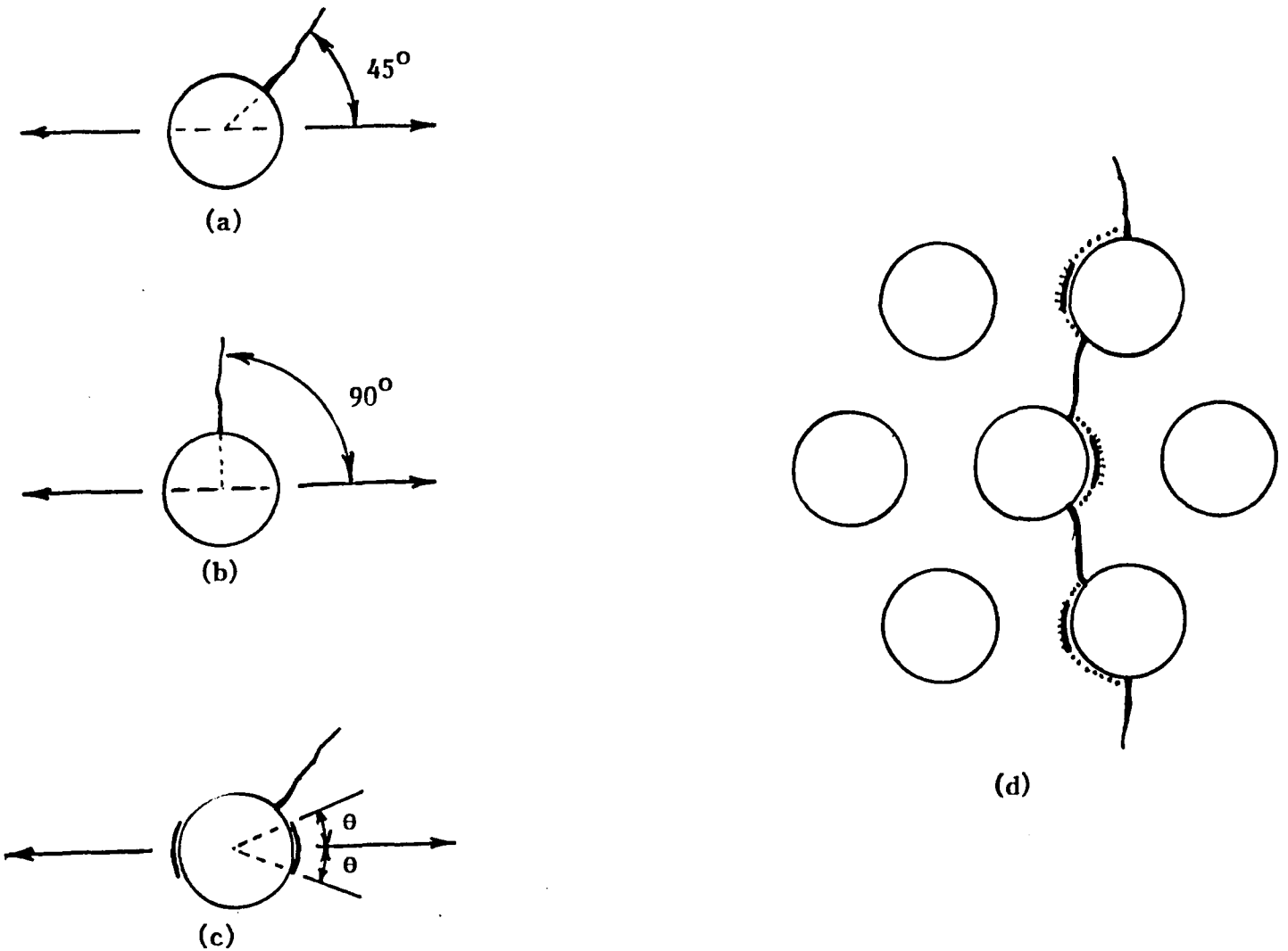

Fig. 7 Developmentof Failure Mechanisms in Transversely Loaded Ceramic Matrix Composite (a) Initial Radial Cracks Around Closely Packed Fibers, (b) Initial Radial Cracks Around Isolated Fibers, (c) Interfacial Cracks, and (d) Interconnection of Radial and Interfacial Cracks

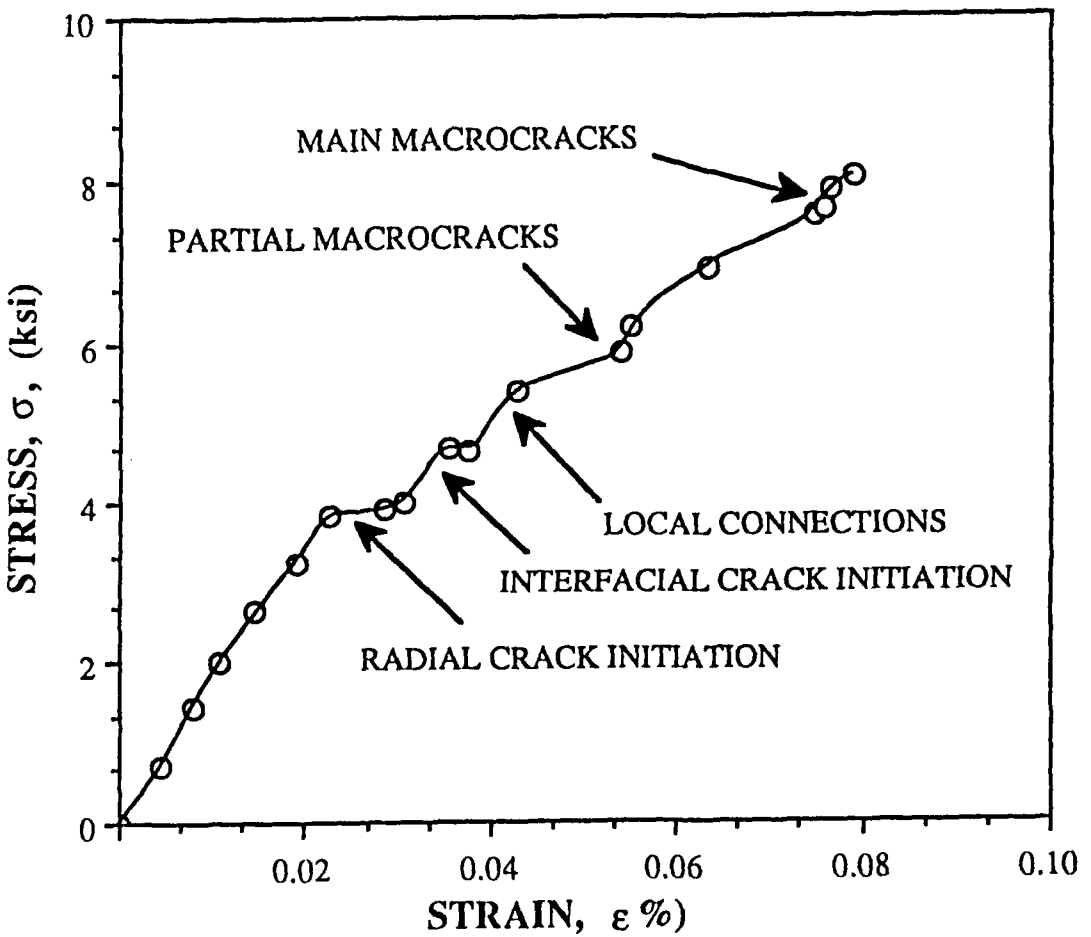

Fig. 8 Stress-Strain Behavior of Crossply Laminate with Corresponding Stages of Damage Development in Transverse Layer

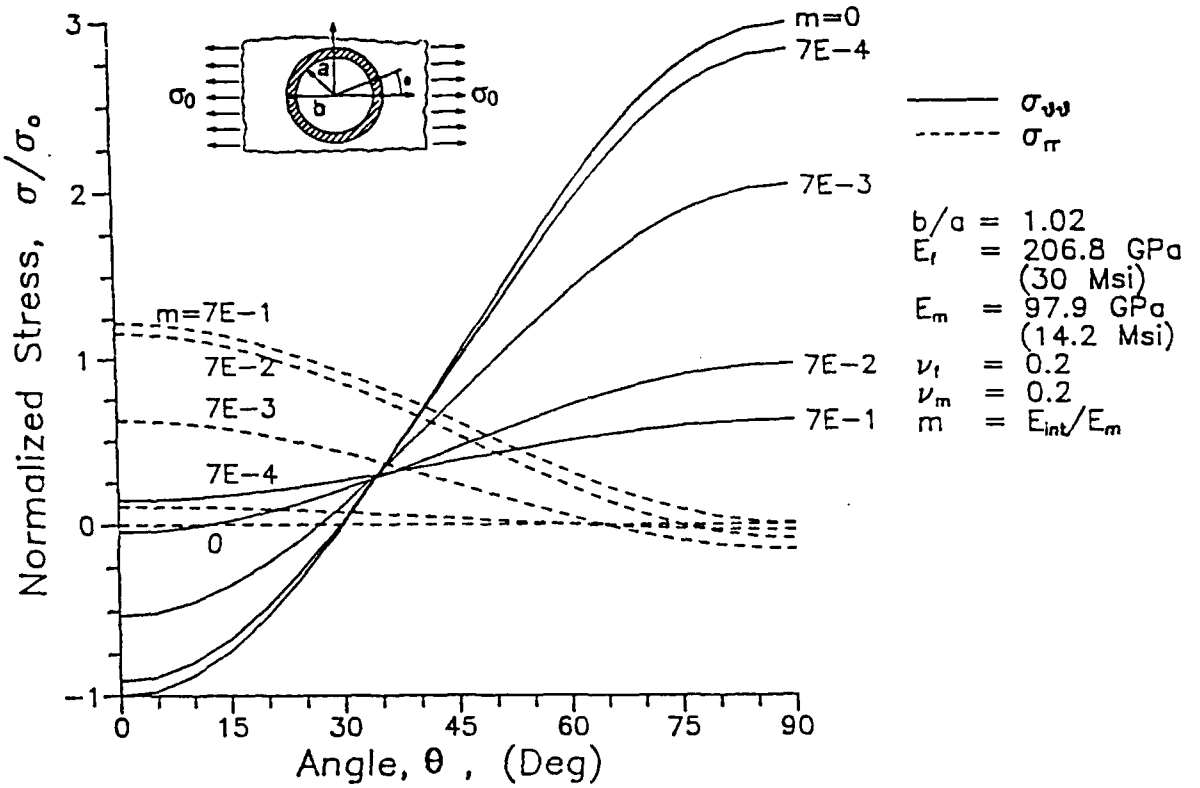

Fig. 9 Elastic analysis of isolated fiber with interphase liner as a function of interphase modulus

location [3]. This of course leads to radial cracking at that location as observed experimentally.

2.4 Investigation of Interphase Stiffness [4]

The elastic analysis discussed before for the case of an isolated fiber was combined with experimental observations to determine the effective stiffness of the interphase. Unidirectional specimens were loaded under the microscope in the transverse to the fiber direction and the applied stress was noted at crack initiation around isolated fibers.

The maximum circumferential stress at $\theta = 90°$ in the matrix is

$$(\sigma_\theta)_{max} = k_\sigma \sigma_o + (\sigma_\theta)_{res} \qquad (1)$$

At failure (radial crack initiation)

$$(\sigma_\theta)_{max} = F_{mT} \qquad (2)$$

$$k_\sigma = \frac{1}{\sigma_o}(F_{mT} - (\sigma_\theta)_{res}) \qquad (3)$$

where

$(\sigma_\theta)_{max}$ = max. circumferential stress at failure

σ_o = applied transverse average stress

k_σ = stress concentration factor

$(\sigma_\theta)_{res}$ = residual circumferential stress

F_{mT} = matrix tensile strength

By noting the applied stress σ_o at crack initiation and knowing the matrix tensile strength F_{mT} and the residual circumferential stress $(\sigma_\theta)_{res}$, we obtain the stress concentration factor k_σ. Figure 10 depicting the variation of stress concentration as a function of interphase modulus, obtained from the results of Fig. 9, is then used to obtain the interphase modulus.

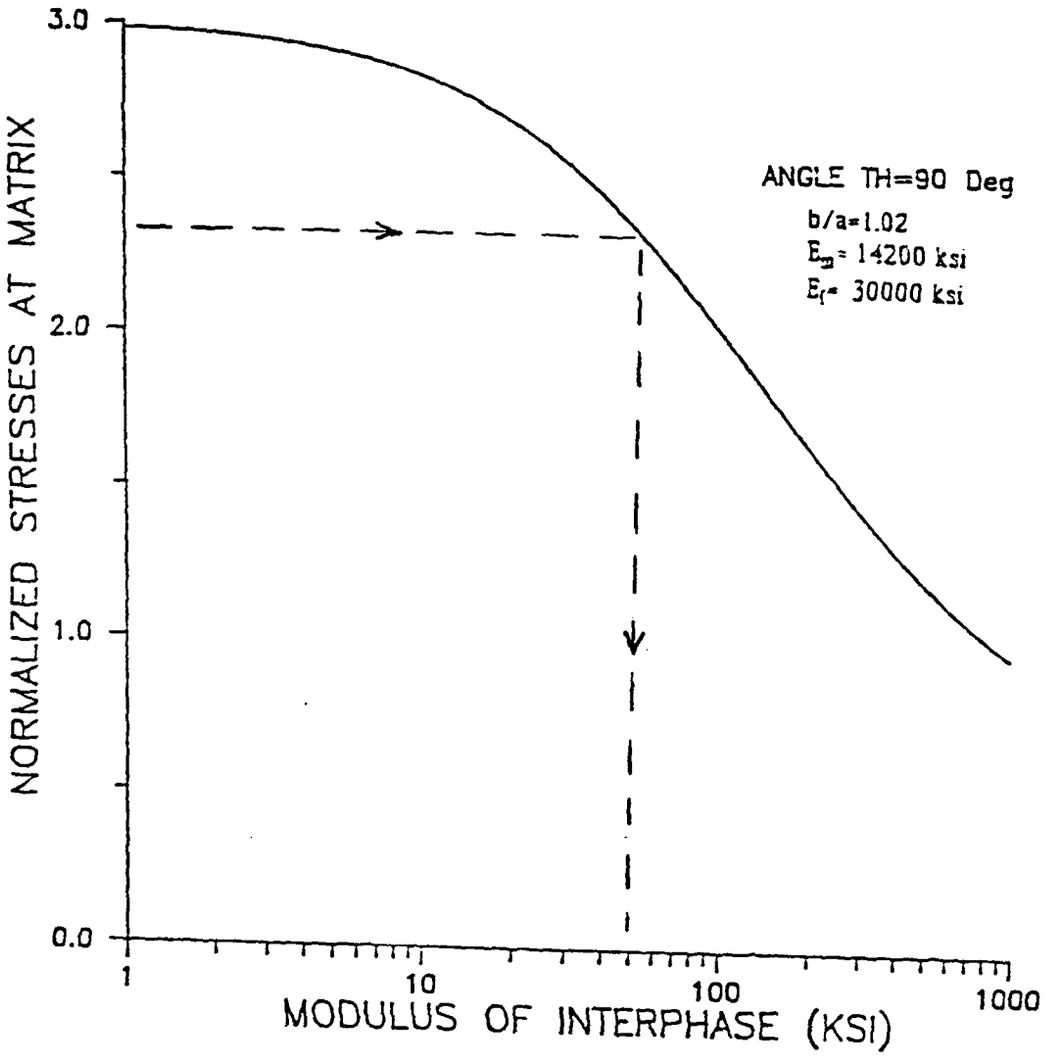

Fig. 10 Variation of the Circumferential Stress in the Matrix at $\theta = 90^{o}$, as a Function of Interphase Modulus

3. ANALYTICAL/EXPERIMENTAL STUDIES OF BRITTLE-MATRIX COMPOSITES UNDER LONGITUDINAL TENSION

A new shear lag model based on a more realistic crack geometry was developed [5]. The model gives closed form solutions for the stresses in the matrix, the fiber and at the interface. It predicts matrix cracking, fiber debonding and overall stress-strain behavior to failure (Fig. 11). At an applied axial stress σ_a, the matrix crack spacing is given by

$$l = \frac{2}{\alpha} \cosh^{-1}\left[\frac{E_m \sigma_a + E_1 \sigma_{rm}}{E_m \sigma_a + E_1 (\sigma_{rm} - F_{mT})}\right] \qquad (4)$$

where E_1 = average longitudinal composite modulus

E_m = matrix modulus

F_{mT} = matrix tensile strength

σ_{rm} = longitudinal matrix residual stress

$$\alpha^2 = \frac{2}{A r_f} \cdot \frac{E_1}{E_f E_m V_m} \qquad (5)$$

$$A = \frac{r_f}{4G_f} + \frac{1}{G_m}\left[\frac{2}{3} \cdot \frac{V_f (r_f - r_m)}{(1 - V_f)^2}\left(4 + \frac{r_f}{r_m} + V_f\right) + \frac{r_f (1 + V_f)}{1 - V_f}\right] \qquad (6)$$

G_f, G_m = fiber and matrix shear moduli, respectively

r_f, r_m = fiber and matrix radii in model, respectively

V_f, V_m = fiber and matrix volume ratios, respectively

The above relation gives the matrix crack spacing as a function of applied stress up to the point of fiber debonding initiation.

The maximum interfacial shear stress τ_i at the crack location is given by

$$\tau_i (0) = \frac{a r_f}{2} \frac{V_m}{V_f}\left(\frac{E_m \sigma_a}{E_1} + \sigma_{rm}\right) \tanh\frac{\alpha l}{2} \qquad (7)$$

When the above shear stress reaches the value of the interfacial shear strength F_{is} debonding occurs and increases with applied stress. Debonding initiation occurs at an applied stress σ_a:

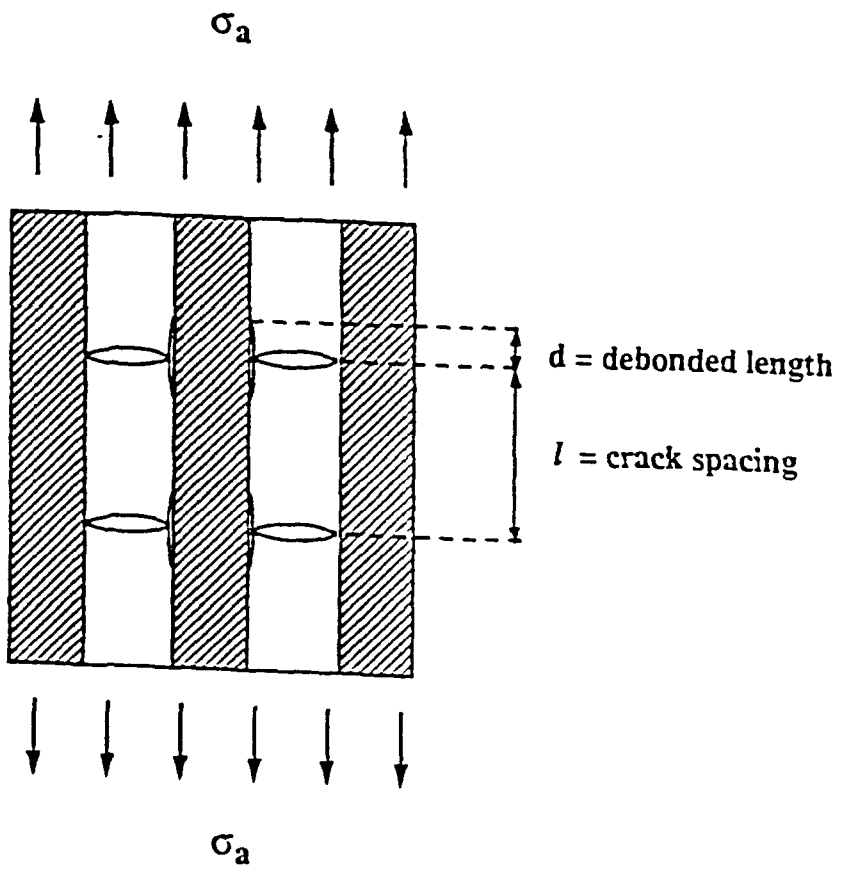

Fig. 11 Matrix Cracking and Debonding in Unidirectional Composite under Longitudinal Tensile Loading

$$\sigma_a = \frac{E_l}{E_m}\left[\frac{2}{\alpha r_f}\frac{V_f}{V_m}\cdot\frac{F_{is}}{\tanh l/2} - \sigma_{rm}\right] \qquad (8)$$

The debonded length was calculated as

$$d = \frac{1}{2}\left[l - \frac{1}{\alpha}\log\frac{1+\xi}{1-\xi}\right] \qquad (9)$$

where

$$\xi = \frac{2F_{is}}{ar_f}\frac{V_f}{V_m}\cdot\frac{E_l}{E_m\,\sigma_a + E_l\,\sigma_{rm}} \qquad (10)$$

The average axial strain in the damaged composite, which is taken to be equal to the average fiber strain, is obtained by calculating the average stress in the fiber and dividing it by the fiber modulus. Thus, a stress-strain relation can be predicted for all stages of damage up to failure.

The theoretical analysis discussed before, subject to the validity of assumptions, can predict transverse matrix crack density, debonded fiber length and average strain in the composite as a function of the applied stress, in terms of geometrical, elastic and strength parameters of the fiber and matrix. These include fiber volume ratio, fiber and matrix moduli and strengths and interfacial shear strength.

In the predictions a matrix tensile strength of 159 MPa (23 ksi) and an interfacial shear strength of 221 MPa (32 ksi) were used and the residual stresses and friction were neglected. The predicted stress-strain, stress versus crack density and stress versus debonded length curves are shown in Fig. 12 and compared with experimental results. The predicted stress-strain curve agrees well with the experimental one initially, but it deviates from it at higher stresses. Possible factors causing this discrepancy are: (1) a degree of random fiber misalignment, (2) some uncertainty of the true effective values of tensile matrix and interfacial shear strengths and (3) the neglect of residual thermal and interface frictional stresses.

The minimum crack spacing predicted by the model is 35 μm which is very close to the measured value of 36 μm. The predicted extent of fiber-matrix debonding at failure is approximately 85%, which is in agreement with experimental evidence of nearly total debonding.

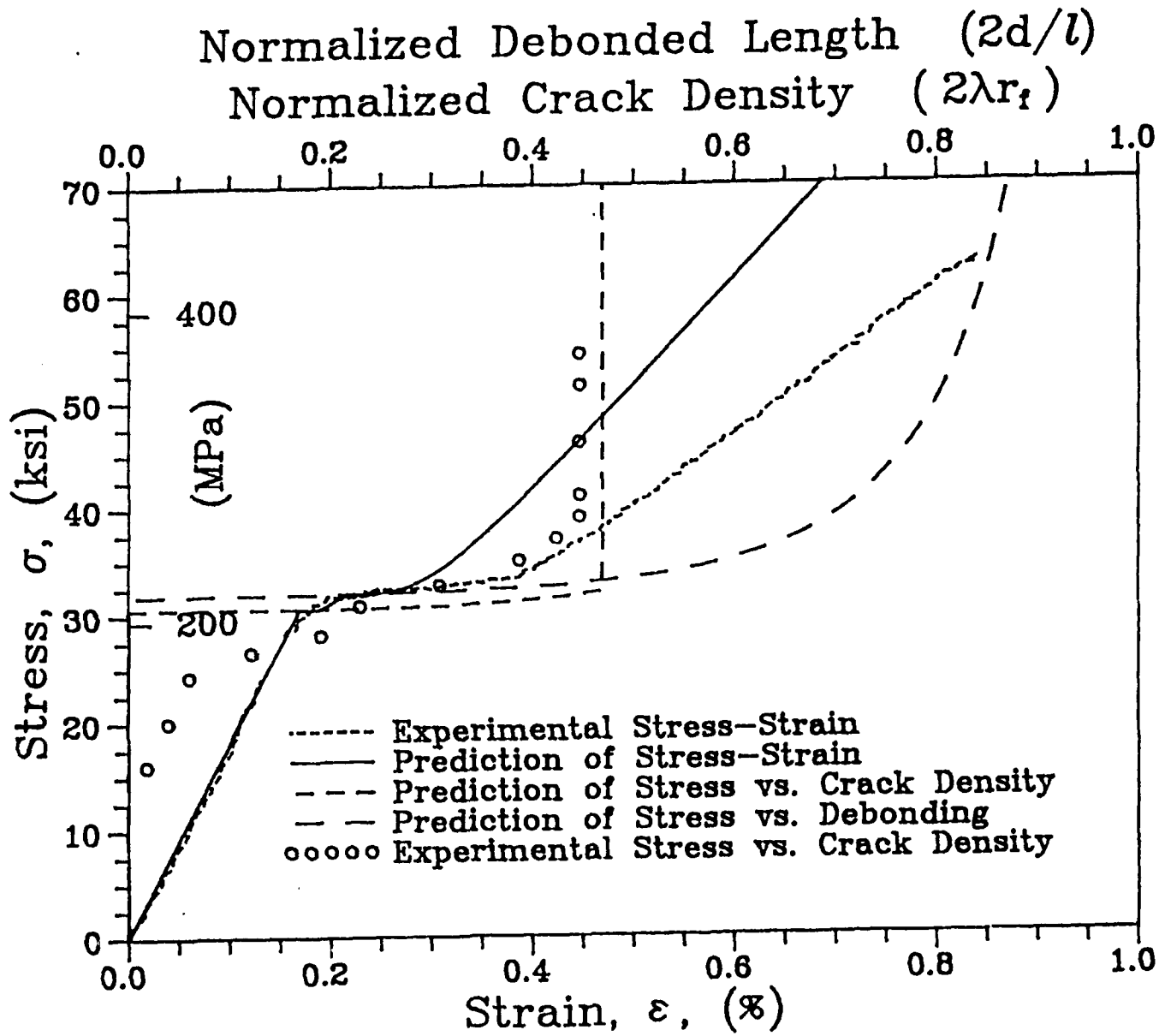

Fig. 12 Stress-Strain, Stress vs. Matrix Crack Density and Stress vs. Debonded Length Curves for SiC/CAS [0$_8$] Unidirectional Composite

4. ANALYTICAL STUDIES OF INTERPHASE EFFECTS IN TRANSVERSELY LOADED COMPOSITE

The effects of compliant interphases on micro-level stresses in a characteristic cell have been calculated for a unidirectionally reinforced composite with rectangular and hexagonal fiber packing under transverse loading. In particular, radial matrix cracking and interphase failure for transverse loading of a hexagonal array fiber composite were investigated by: (1) modeling the interphase by a layer of radial and circumferential spring elements, (2) adopting a tensile stress criterion for initiation of matrix cracking, and (3) employing a strain-energy density criterion for interphase failure. The mechanical behavior of the composite was defined in terms of geometrical, stiffness and strength parameters. Stresses on the microlevel were calculated. Under the assumption that the failure mechanisms follow the periodicity of the composite, two scenarios related to different values of the strength parameters were investigated. In the first scenario matrix cracking occurs first, followed by interphase failure. In the second scenario interphase failure is followed by matrix cracking. Typical results were reported in Refs. [3, 6-9].

The work that has been completed shows that the mechanical properties of fiber-matrix interphases significantly affect the overall stiffness and strength of a fiber-reinforced composite. For a quantitative analysis an interphase can be modeled in two ways. In a first model the interphase is considered as a thin annular layer in between the fiber and the matrix, with mechanical properties that differ from those of both the fiber and matrix materials. A number of authors have pursued this approach for a single fiber in an unbounded matrix. The thin annular layer model introduces at least three parameters, namely, the thickness of the interphase and two elastic constants. These parameters are generally very difficult to obtain. The model gives also rise to significant analytical complications when closely spaced fibers are considered and mechanical interactions between the fibers cannot be neglected.

The number of parameters can be reduced to two and the analytical complications can be decreased by what amounts to an averaging procedure across the thickness of the annular layer. In that manner, the thickness and the elastic constants are combined into two spring constants. This simplified model can also be used if the condition between the fiber and the matrix is of the nature

of contact between rough surfaces containing microcracks, voids and asperities. The spring-layer has also been used by a number of authors. The relation between the spring constants and the parameters of an annular interphase layer has also been discussed.

The compliant interphase zone between fibers and matrix was represented by a spring-layer model. With respect to local polar coordinates the relations between the relevant stress and displacement components may then be expressed as

$$\sigma_r^m = \sigma_r^f = k_r\left(u_r^m - u_r^f\right), \qquad \text{if } u_r^m \geq u_r^f \tag{11}$$

$$\sigma_r^m = \sigma_r^f \text{ and } u_r^m - u_r^f, \qquad \text{if } u_r^m > u_r^f \tag{12}$$

and

$$\sigma_{r\theta}^m = \sigma_{r\theta}^f = k_\theta\left(u_\theta^m - u_\theta^f\right) \tag{13}$$

where σ_r is the interfacial radial stress, $\sigma_{r\theta}$ is the interfacial shear stress, and u_r and u_θ are the displacements in the radial and the circumferential direction, respectively. Quantities with upper index 'm' and 'f' are defined in the matrix and the fiber regions, respectively. The constants k_r and k_θ are the coefficients of the springs. The addition of Eq. (12) insures that the model will not allow an unrealistic radial overlap of the two materials in the interfacial zone.

It is noted that the compliant conditions (11) - (13) include the case of perfect contact ($k_r = \infty$, $k_\theta = \infty$), when the stresses and displacements are continuous, and the case of no contact ($k_r = k_\theta \equiv 0$) when the stresses vanish. It is also noted that for a disbond the ligament at the tip of the disbond undergoes a finite stretch when in tension, and consequently the stress remains bounded. Hence the usual problems of violently oscillating singularities that are associated with crack-tip fields for a crack in a perfectly bonded interface, do not occur for the spring-layer model.

Taking advantage of the periodicity of the medium, the states of stress and deformation in a basic cell were analyzed numerically by means of the boundary element method. The circumferential tensile stress along the matrix side of the interphase and the radial stress in the interphase were analyzed for various values of the interphase parameters and fiber volume ratio.

Two important conclusions verified experimentally are illustrated in Figs. 13 and 14. Figure 13 shows the influence of fiber volume ratio on the distribution of the circumferential stress in the matrix. It shows that as the fiber volume increases, i.e., as the fiber packing gets denser, the maximum circumferential stress moves from the 90° location towards the 45° location. Furthermore, for a fixed fiber volume ratio, the same trend occurs as the interphase modulus decreases (Fig. 14). The micromechanical results were also used to determine the effect of interphase stiffness on the effective moduli. The calculated values were compared with analytical results that were adjusted for interphase stiffness. Stresses on the microlevel were calculated for the trapezoidal element shown in Fig. 15.

An investigation of the initiation and propagation of matrix cracks and interphase disbonds must be based on appropriate criteria. Let us first consider the initiation of matrix cracks. For a perfect composite subjected to tensile stresses, numerical results show, in agreement with physical intuition, that the circumferential tensile stress at the fiber matrix interphase is the largest tensile stress component in the matrix material. As a crack initiation criterion we therefore choose

$$\sigma_\theta \geq \sigma_\theta^{cr} \tag{14}$$

On the basis of Eq. 14, it is assumed that, in agreement with experimental observations [1,2], a radial matrix crack is formed at the interphase when Eq. (14) is satisfied. It is assumed that the propagation of such a crack is governed by the fracture toughness, K_I^{cr}. Indeed, it turns out that for the far-field transverse tensile loading which is being considered here, the mode-II stress intensity factor is negligible as compared to K_I. Hence we consider as condition for continued radial matrix cracking that

$$K_I \geq K_I^{cr} \tag{15}$$

A typical stress-strain curve for the first scenario is shown in Fig. 16 and compared in insert with the experimentally obtained curve.

For the generation of disbonds, as well as their propagation and arrest, it is feasible to use such criteria as critical stress, critical strain or critical strain energy density, because in the spring-layer model all these quantities are well defined near the tip of a disbond. In this work we have

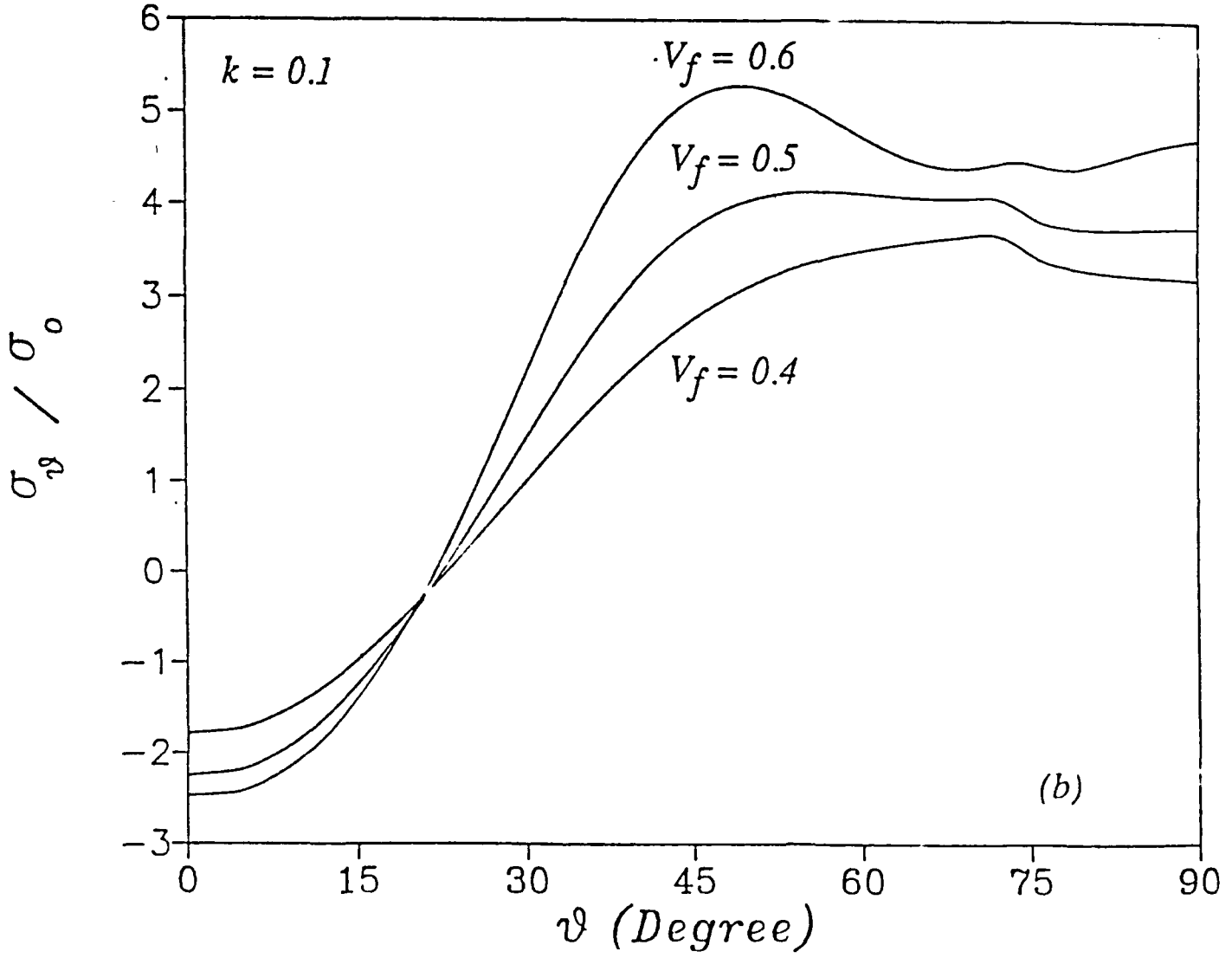

Fig. 13 Circumferential Tensile Stress, σ_ϑ, at the Matrix Side of the Interphase for Various Fiber Volume Ratios

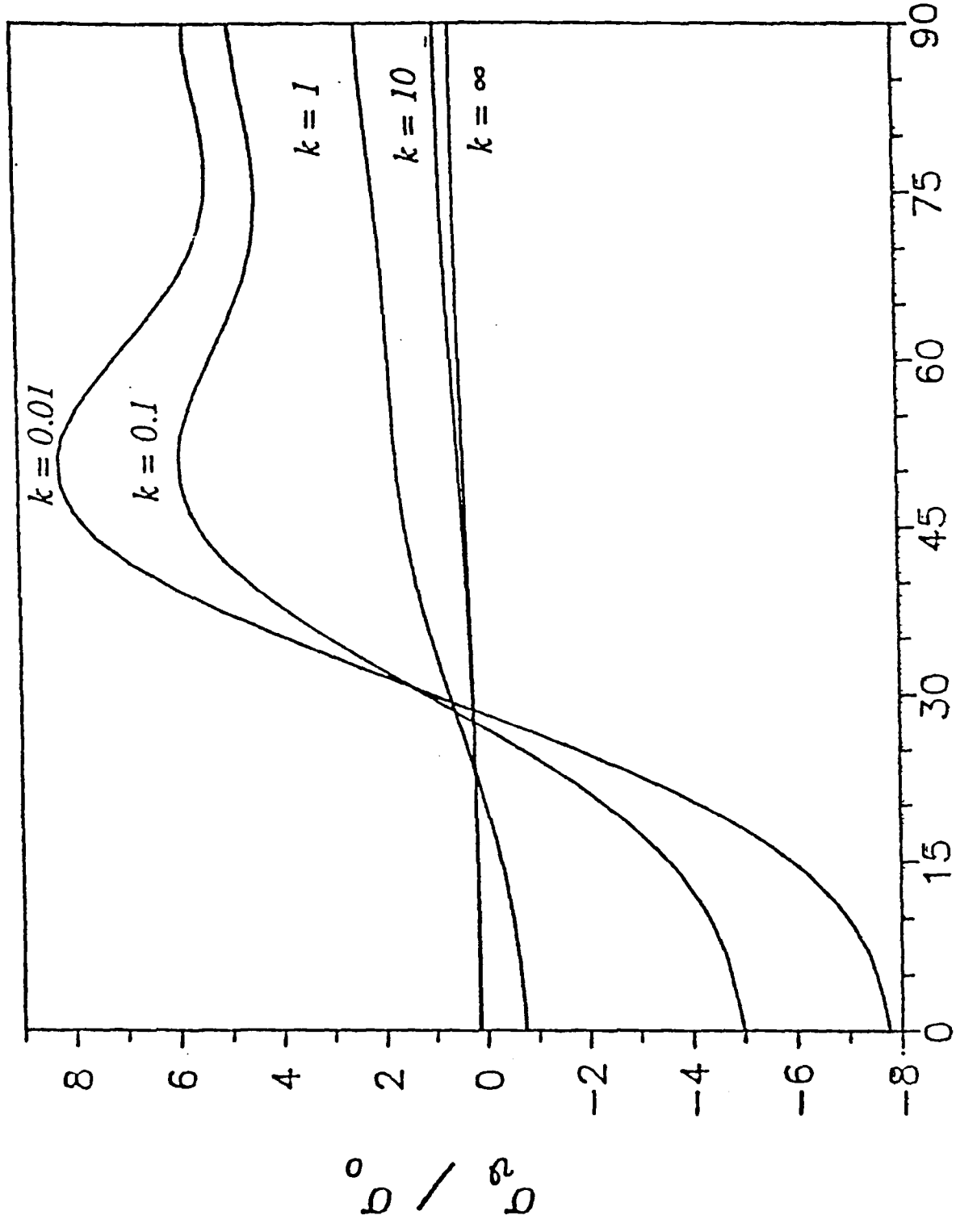

Fig. 14 Circumferential Stress, σ_θ, at the Matrix Side of the Interphase for Various Interphase Stiffnesses

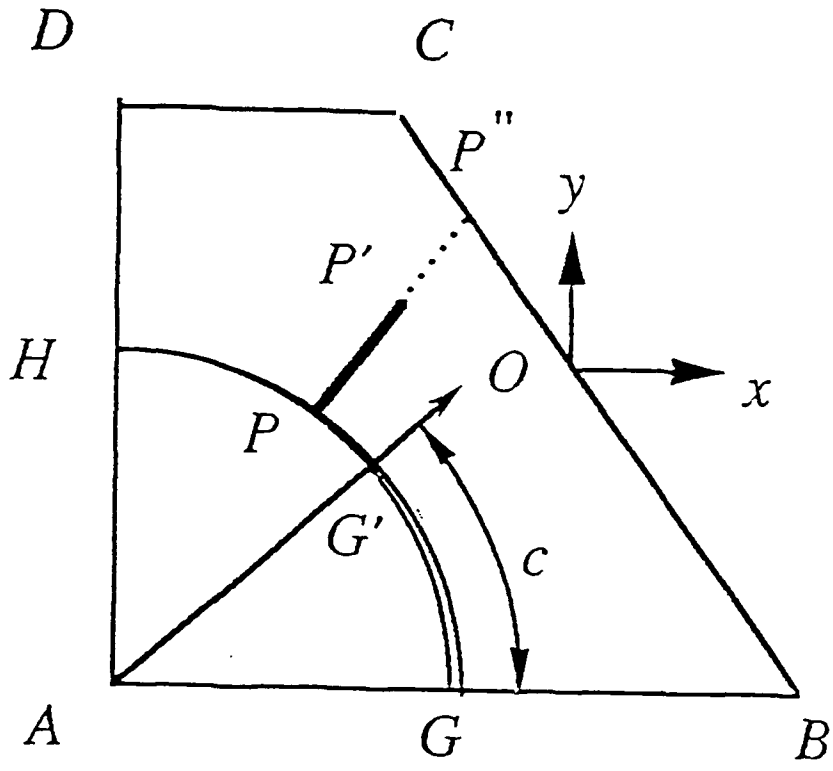

Fig. 15 Trapezoidal Domain with Radial Matrix Crack and Interphase Disbond

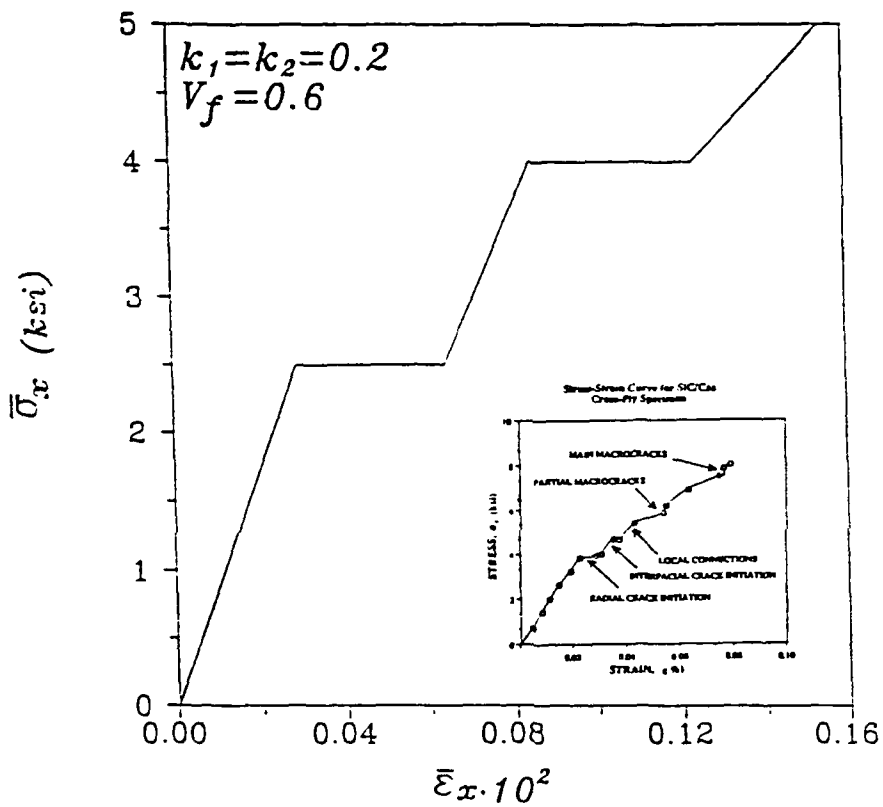

Fig. 16 **Effective Stress-Strain Relation When Radial Matrix Cracking is followed by Interphase Disbonding**

employed an energy density criterion, since it combines information on the tensile and shear stresses in the interphase. The strain energy per unit interphase area is easy to calculate. We have

$$U = \frac{\sigma_r^2}{2k_r} + \frac{\sigma_{r\theta}^2}{2k_\theta} \tag{16a}$$

It is assumed that the interphase will break and form a disbond when

$$U > U^{cr} \tag{16b}$$

There are many material and geometrical parameters in the problem at hand. They may be summarized as follows. Material parameters: shear moduli, Poisson's ratios, interface stiffnesses, critical stress for matrix crack initiation, fracture toughness of matrix material, critical value of interphase strain energy density. Loading parameters: far-field (transverse) stress. Geometrical parameters: fiber radius, fiber-center spacing, fiber volume density, half-length of interphase disbond, length of radial matrix crack. Numerical results for the fields of stress and deformation in the trapezoidal cells have been obtained by the use of the boundary element method.

5. FAILURE MODELS FOR UNIDIRECTIONAL COMPOSITES UNDER LONGITUDINAL TENSION

Matrix fracture of a brittle matrix composite under longitudinal tension was analyzed for the case when the fracture strain of the fiber is larger than that of the matrix. An hexagonal array of fibers was assumed. The axisymmetric problem of an infinitely long elastic fiber perfectly bonded to an elastic matrix cylinder containing an annular crack surrounding the fiber was considered first for the case of uniform longitudinal strain (Fig. 17) [10,11]. Displacements and stresses were expressed in terms of Love's stress function. Boundary conditions used were continuity of displacements and stresses at the interface and stress-free conditions at the crack face and the outer boundary of the matrix cylinder. The problem was formulated in terms of a singular integral equation with a Cauchy type kernel which was solved numerically. When the inner crack tip terminates at the interface, it was shown that the characteristic equation is the same as that for the case of plane strain. Four possible crack configurations are considered as follows: (a) Internal

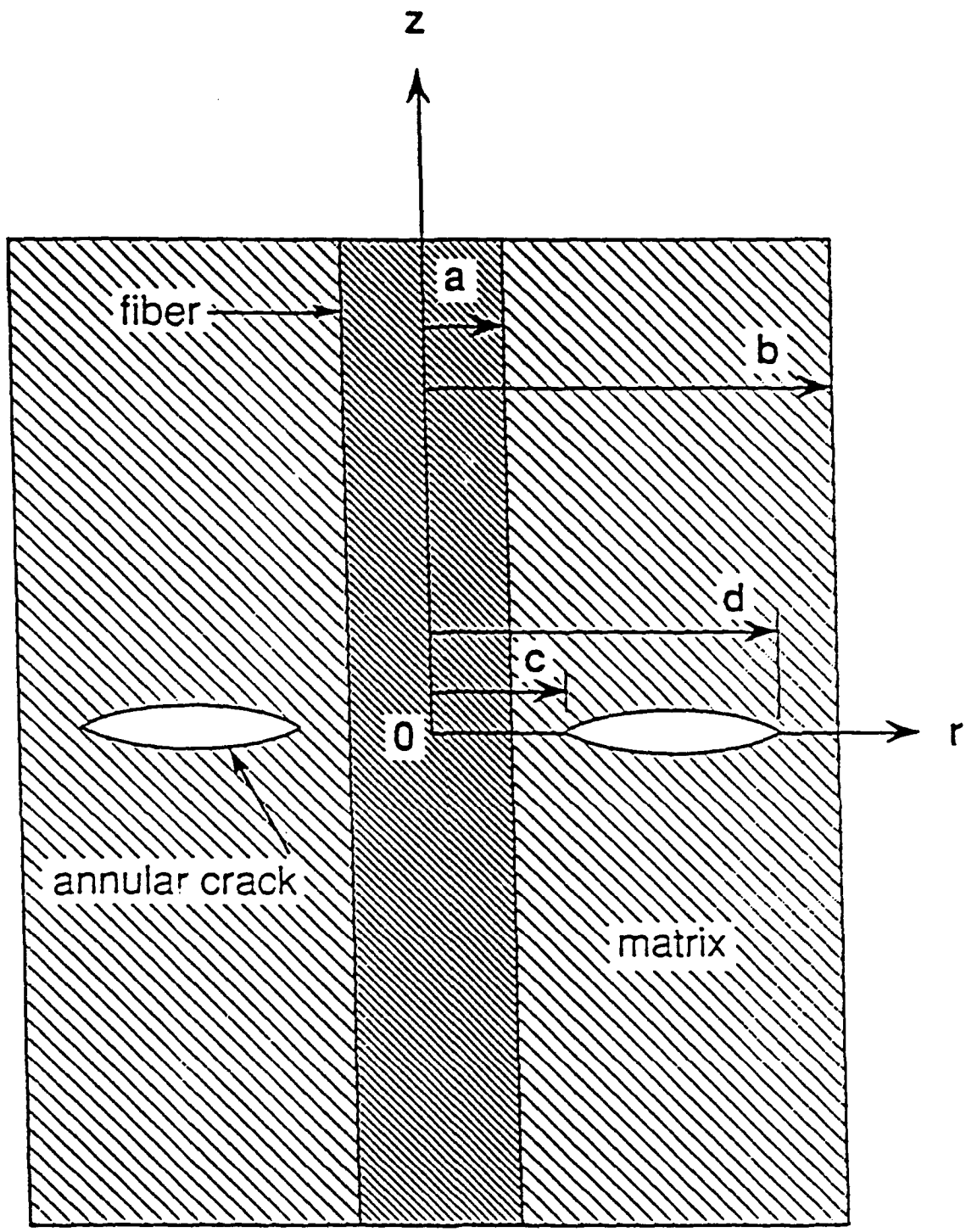

Fig. 17 An annular matrix crack surrounding the elastic fiber. Approximation to the case of a hexagonal array of fibers in a matrix where the concentric circular cylinder model represents a unit cell.

annular crack with inner crack tip away from the interface. (b) Internal annular crack with inner crack tip at the interface. (c) Annular edge crack with inner crack tip away from the interface. (d) Annular edge crack with inner crack tip at the interface (fully cracked matrix). Stress intensity factors were given for a wide range of crack sizes for different ratios of shear moduli. Stress fields were presented for a typical brittle matrix fiber-reinforced composite, SiC/CAS calcium aluminosilicate glass ceramic reinforced with silicon carbide fibers.

The case of an annular edge crack terminating at the interface was given particular attention (Fig. 18). Normalized stresses along the interface are plotted in Fig. 19 and normalized axial and shear stresses along the radial direction at a distance b/2 from the crack are plotted in Fig. 20.

Multiple cracking in a fiber-reinforced brittle matrix composite under longitudinal tensile loading was investigated within the framework of linear elastic fracture mechanics (Fig. 21) [12]. Stress intensity factors were obtained for different ratios of shear moduli, crack spacings and fiber volume fractions. Stress fields were given for a brittle matrix fiber-reinforced composite, calcium aluminosilicate glass ceramic reinforced with silicon carbide fibers (SiC/CAS). The stress fields are used to predict damage mechanisms in the composite. It is shown that crack interaction effects are significant for crack spacings that are observed in composites with good bonding at the fiber-matrix interface.

6. PROPOSED FUTURE WORK

It is recommended that the work reported here be continued along the following directions:

1. Further investigation of failure processes of unidirectional ceramic-matrix composite under longitudinal tension. This should include systematic testing to detect and monitor the initiation and development of all failure mechanisms, including matrix cracking, fiber-matrix debonding and fiber fractures. The modified shear lag analysis discussed here should be extended to account for residual stresses and interfacial friction following fiber matrix debonding.

2. Characterization of interphase and its effects on toughness and failure of unidirectional composites under longitudinal and transverse tension.

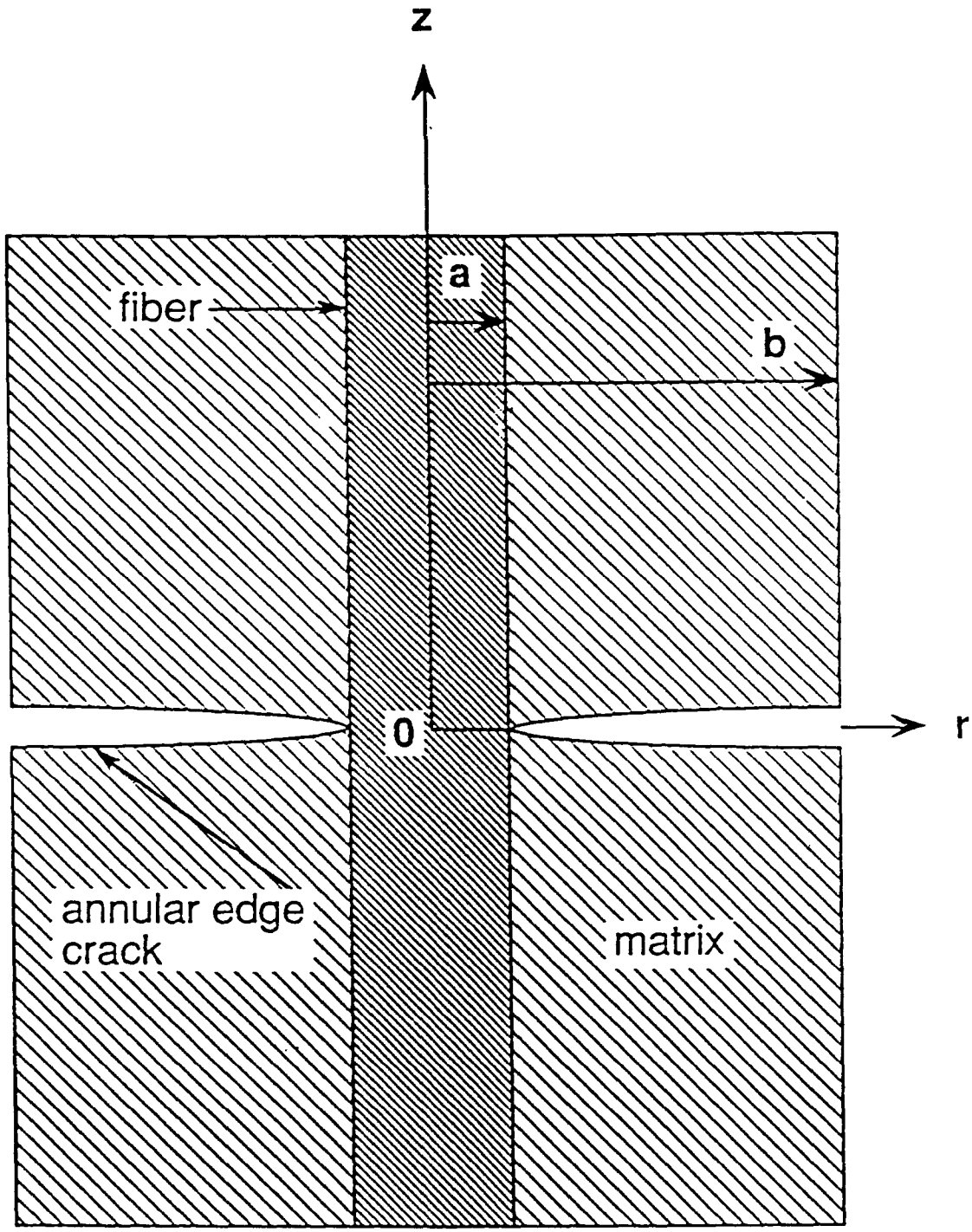

Fig. 18 Annular edge crack with inner crack tip at the interface (fully cracked matrix)

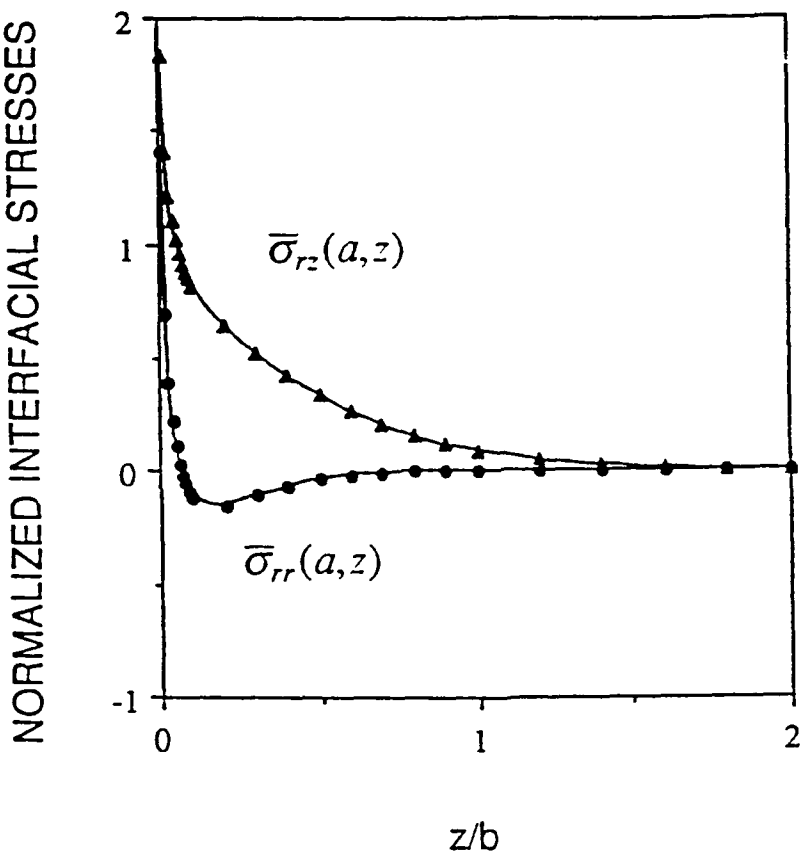

Fig. 19 **Normalized Stresses Along Fiber-Matrix Interface**

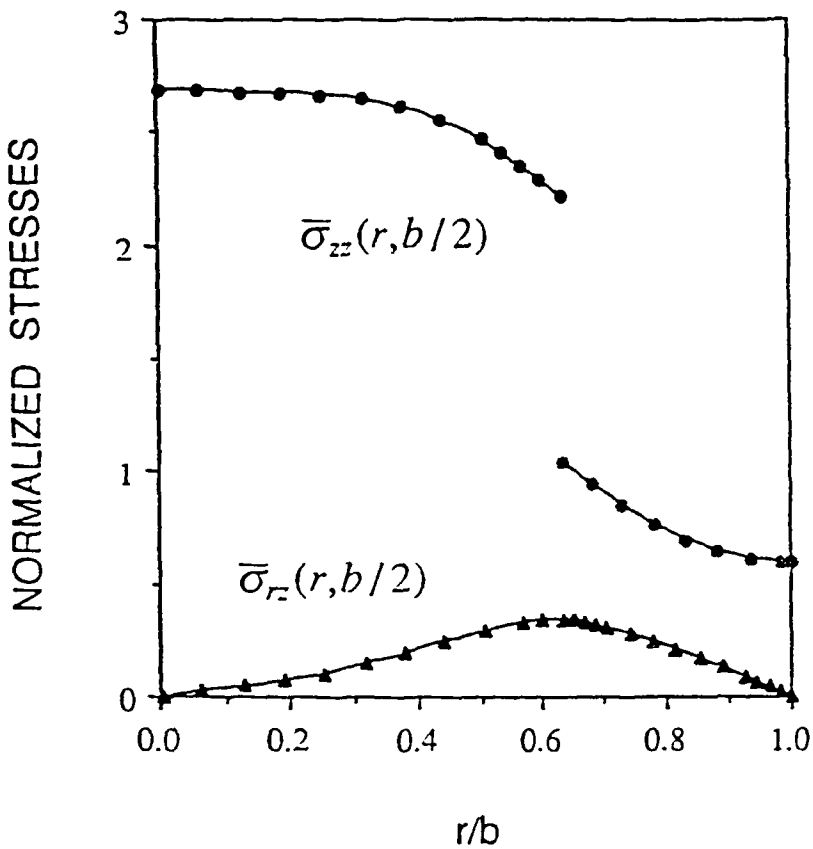

Fig. 20 **Normalized Stresses in Fiber and Matrix Along Radial Direction at Distance b/2 from Crack Face**

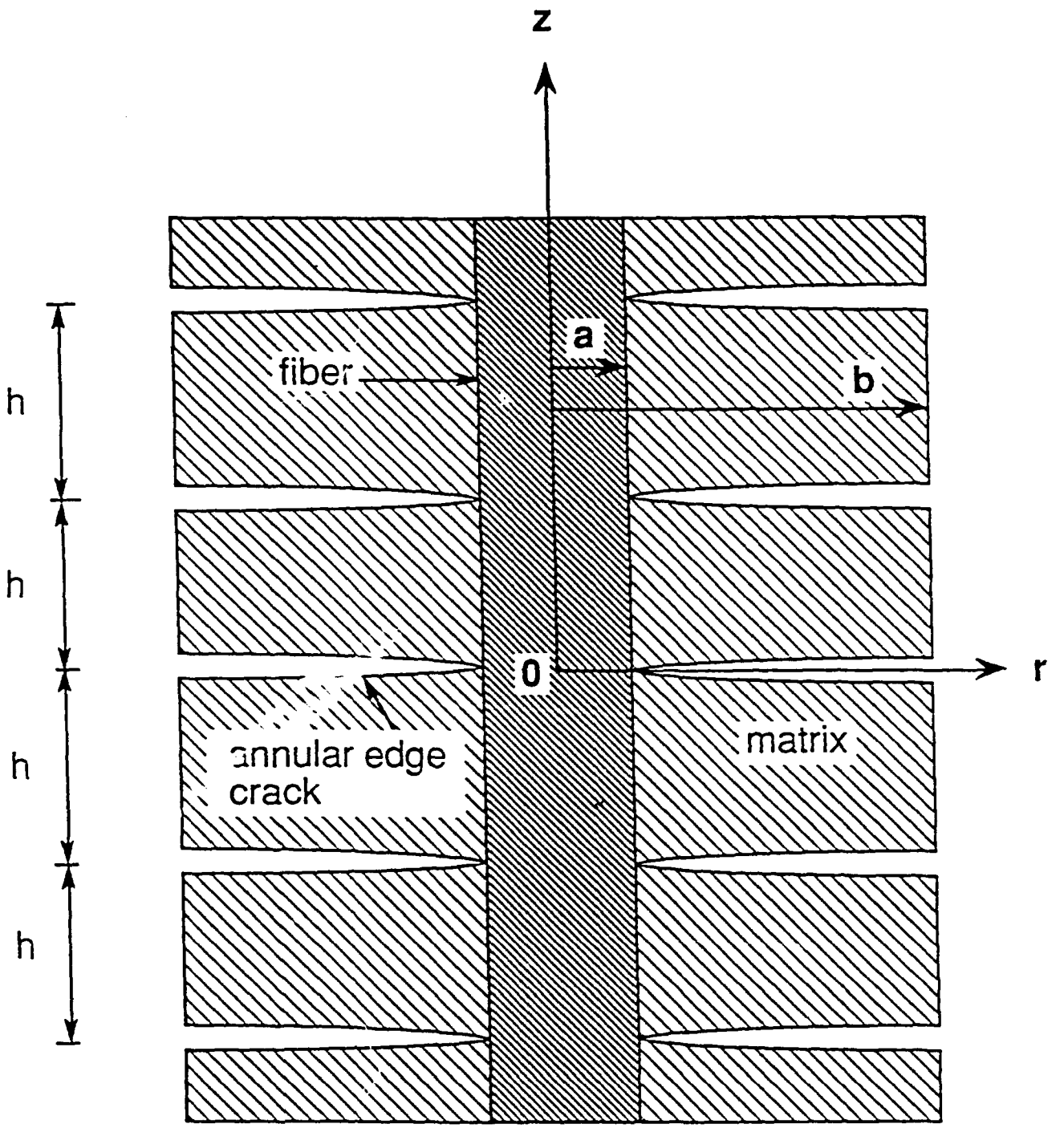

Fig. 21 Periodic Array of Annular Edge Cracks

Analytical studies of the effects of the interphase zone should be extended to account for interactions of radial and interface cracks and to the effects of fiber-matrix defects in an isolated fiber on the stress states of neighboring fibers.

3. Deformation and failure of unidirectional composite under in-plane shear (torsion).

4. Determination of processing residual stresses and their influence on overall behavior of composite.

This study should combine experimental and analytical methods including micro- and macromechanical approaches. This study could be combined with that of material behavior at elevated temperatures.

5. Study of deformation and failure processes in crossply ceramic matrix composites.

Here, the interaction of failure mechanisms in the 90° and 0° layers might be of great interest. The analysis of the effects of the interphase should be extended to the case of a crossply laminate.

REFERENCES

1. I. M. Daniel, G. J. Anastassopoulos and J.-W. Lee, "Failure Mechanisms in Ceramic Matrix Composites," Proceedings of the Society for Exper. Mechanics, May 1989, pp. 832-838.

2. I. M. Daniel, G. J. Anastassopoulos and J.-W. Lee, "Experimental Micromechanics of Brittle-Matrix Composites," ASME, Symposium on Micromechanics: Experimental Techniques, AMD-Vol. 102, W. N. Sharpe, Jr. ed., ASME, 1990, pp. 133-146.

3. J. D. Achenbach and H. Zhu, "Effect of Interphases on Micro and Macromechanical Behavior of Hexagonal-Array Fiber Composites," J. Applied Mechanics, Vol. 57, Dec. 1990, pp. 956-963.

4. G. J. Anastassopoulos and I. M. Daniel, "Investigation of Interphase Stiffness in a Ceramic Matrix Composite," Proc. of Third International Symposium, Advanced Composites in Emerging Technologies, Patras, Greece, Aug. 1990.

5. J.-W. Lee and I. M. Daniel, "Deformation and Failure of Longitudinally Loaded Brittle-Matrix Composites," presented at ASTM Conf. on Composite Materials: Testing and Design, Apr. 1990, (to be published in ASTM STP).

6. J. D. Achenbach and H. Zhu, "Effect of Interfacial Zone on Mechanical Behavior and Failure of Fiber-Reinforced Composites," J. Mech. Phys. Solids, Vol. 37, No. 3, 1989, pp. 381-393.

7. H. Zhu and J. D. Achenbach, "Effect of Fiber-Matrix Interphase Defects on Microlevel Stress States at Neighboring Fibers," J. Composite Materials, Vol. 25, March 1991, pp. 224-238.

8. H. Zhu and J. D. Achenbach, "Radial Matrix Cracking and Interphase Failure in Transversely Loaded Fiber Composites," to be published in Mechanics of Materials.

9. H. Zhu and J. D. Achenbach, "Matrix Cracks and Interphase Failure in Transversely Loaded Fiber Composites," Proc. 22nd National Symposium on Fracture Mechanics, ASTM Special Technical Publication, forthcoming.

10. A. C. Wijeyewickrema, K. Hirashima, L. M. Keer, and T. Mura, "The Annular Crack Surrounding an Elastic Fiber in a Tension Field," Int. J. of Solids and Structures, Vol. 27, No. 3, 1991, pp. 315-328.

11. A. C. Wijeyewickrema and L. M. Keer, "Matrix Fracture in Brittle Matrix Fiber Reinforced Composites," Int. J. of Solids and Structures, 1991.

12. A. C. Wijeyewickrema and L. M. Keer, "Matrix Crack Interaction in a Fiber-Reinforced Brittle Matrix Composite," Int. J. of Solids and Structures, under review.